Applied Physics Letters

RESEARCH ARTICLE | JUNE 13 2023

Optical grade bromide-based thin film electrolytes

Nicola Melchioni ; Giacomo Trupiano ; Giorgio Tofani ; Riccardo Bertini ; Andrea Mezzetta ; Federica Bianco ; Lorenzo Guazzelli ; Fabio Beltram ; Christian Silvio Pomelli ; Stefano Roddaro ; Alessandro Tredicucci ; Federico Paolucci

Appl. Phys. Lett. 122, 243505 (2023)
https://doi.org/10.1063/5.0153394

AIP Publishing

Applied Physics Letters ARTICLE pubs.aip.org/aip/apl

Optical grade bromide-based thin film electrolytes

Cite as: Appl. Phys. Lett. **122**, 243505 (2023); doi: 10.1063/5.0153394
Submitted: 7 April 2023 · Accepted: 1 June 2023 ·
Published Online: 13 June 2023

Nicola Melchioni,[1,2,a)] Giacomo Trupiano,[1,2] Giorgio Tofani,[2,3] Riccardo Bertini,[2] Andrea Mezzetta,[3] Federica Bianco,[1] Lorenzo Guazzelli,[3] Fabio Beltram,[1] Christian Silvio Pomelli,[3] Stefano Roddaro,[2] Alessandro Tredicucci,[1,2] and Federico Paolucci[1,4,b)]

AFFILIATIONS

[1]NEST Laboratory, Istituto Nanoscienze CNR and Scuola Normale Superiore, Piazza San Silvestro 12, I-56127 Pisa, Italy
[2]Dipartimento di Fisica "E. Fermi," Università di Pisa, Largo Bruno Pontecorvo 3, I-56127 Pisa, Italy
[3]Dipartimento di Farmacia, Università di Pisa, Via Bonanno 33, 56126 Pisa, Italy
[4]INFN Sezione di Pisa, Largo Bruno Pontecorvo 3, I-56127 Pisa, Italy

[a)]Author to whom correspondence should be addressed: nicola.melchioni@sns.it
[b)]Electronic mail: federico.paolucci@pi.infn.it

ABSTRACT

Controlling the charge density in low-dimensional materials with an electrostatic potential is a powerful tool to explore and influence their electronic and optical properties. Conventional solid gates impose strict geometrical constraints to the devices and often absorb electromagnetic radiation in the infrared (IR) region. A powerful alternative is ionic liquid (IL) gating. This technique only needs a metallic electrode in contact with the IL, and the highest achievable electric field is limited by the electrochemical interactions of the IL with the environment. Despite the excellent gating properties, a large number of ILs are hardly exploitable for optical experiments in the mid-IR region because they typically suffer from low optical transparency and degradation in ambient conditions. Here, we report the realization of two electrolytes based on bromide ILs dissolved in polymethyl methacrylate (PMMA). We demonstrate that such electrolytes in the form of thin films can induce state-of-the-art charge densities as high as 20×10^{15} cm^{-2} with an electrochemical window of [−1V, 1V] in vacuum. Thanks to the low water absorption of PMMA, they work both in vacuum and in ambient atmosphere after a simple vacuum curing. Furthermore, our electrolytes can be spin-coated into flat thin films with optical transparency in the range from 600 to 4000 cm^{-1}. Thanks to these properties, these electrolytes are excellent candidates to fill the gap as versatile gating layers for electronic and mid-IR optoelectronic devices.

The possibility of controlling the charge density in an electron gas with electrostatic potentials (field-effect) unlocked many technologies at the basis of modern life. Such field-effect found renewed importance in experiments involving low-dimensional systems, such as 2D materials, van der Waals heterostructures, and nanowires. In those materials, a modification of the electronic density can have great impact on charge transport and infrared (IR) optical response.[1,2] Moreover, field-effect dramatically influences the band structure of 2D crystals,[3–8] since their few-atomic thickness prevents an efficient screening of the electric field created by the gate electrode. Conventionally, different solid-gate geometries are exploited, such as highly doped substrates covered with a dielectric (back-gate[9]), a dielectric deposited on the crystal hosting an electrode on top (top-gate[4]), lateral metallic pads on the same insulating substrate (side-gate[10]), or even van der Waals heterostructures, where different layers act as gate electrode, dielectric, and channel medium.[11] When dealing with optical experiments involving 2D materials and bulk semiconductors, such geometries are a limitation. Indeed, the high dielectric losses hinder the back-gating efficiency of the substrate, and a top-gate would prevent adequate optical transparency, while side-gates do not grant the necessary spatial uniformity in the achievable charge density.

In this framework, ionic liquids (ILs) could be a versatile tool to overcome these restrictions. Indeed, ILs work independently from the surrounding environment and need only to be electrically contacted, thus being employable on fully insulating substrates and several gating geometries.[12–15] In the presence of a voltage between the channel and the gate electrode, the ions inside the IL arrange as charged layers at their surfaces. The electrostatic potential created by these ionic layers is screened by the attraction of charge carriers (electrons or holes) inside the channel and the gate electrode, thus forming the so-called electric double layers (EDLs).[16] These EDLs are parallel plate capacitors with inter-plate distance of a few nm, thus offering an enhanced gating efficiency due to their high capacitance.[17–19] The generated electric fields up to 10 GV/m[20] allowed to explore unprecedented regimes,

where deep modifications to the electronic properties were induced.[21–24] Moreover, while the dielectric breakdown restricts the efficiency of solid-state gates,[25,26] the main limitation of electrolyte gating is the electrochemical interaction of the IL with the surrounding environment.[27] For example, despite their high ionic transport efficiency, lithium-based electrolytes are expensive, highly reactive with most of other chemical substances[28] and scarcely compatible with polymer matrices. Differently, bromide-based ILs are widely available at accessible costs, polymer compatible, and, at the same time, thermally and electrochemically stable.[29,30] However, most commercially available compounds are unstable under high voltage bias and exhibit poor transparency in the IR region.[31–33]

In this Letter, we present the development of two IR-transparent polymer electrolytes based on bromide ionic liquids (Br-ILs) dissolved in polymethyl methacrylate (PMMA). To this scope, we study their optical and charge transport properties when they are spin-coated onto a substrate to form a thin film. In particular, we show that our electrolytes have large windows with $<0.007\ \mu m^{-1}$ absorption in the range from 600 to 4000 cm^{-1} in air and are able to induced charge densities up to $\sim 20 \times 10^{15}\ cm^{-2}$ in vacuum. Since their fabrication does not impose any geometrical restriction, our electrolytes can be employed as versatile transparent gates for low-dimensional materials in optical and optoelectronic experiments in the IR region. In addition, thanks to the flat surface, such electrolytic films might be an easily accessible key element for a wide variety of experiments, such as light-matter interaction studies on mixed 2D-bulk semiconductor structures or double-gated systems at extreme charge concentrations.

We first focus on the IR optical response and transport properties of two pure bromide-based ionic liquids (ES1 and ES2). ES1 is commercial tetraoctylphosphonium bromide [$P(C8)_4Br$] of purity >95%, while ES2 is 3,3′-(hexane-1,6-diyl)bis(1-methyl-1*H*-imidazolium)bromide [$C_6(MIM)_2$/2Br 3C6 Br]. ES2 was synthesized using the standard ionic liquid synthesis procedure[34] adapted for dicationic ionic liquids.[29] A solution (2.1 equiv : 5 ml) of 1-methylimidazole (98%) in acetonitrile (≥99%) was added dropwise under magnetic stirring to a solution (2 g, 1 equiv) of 1,6-dibromohexane (98%) in 10 ml of acetonitrile. The solution was stirred for 2 min, and then the mixture was heated up and stirred at 80 °C for 48 h. A white solid precipitation was observed after half an hour. The solvent was removed under reduced pressure, and the obtained solid was washed three times with 10 ml of diethyl ether (99%+) and dried *in vacuo* at 65 °C.

To determine the IR optical properties of ES1 and ES2, two solid samples of the ILs were measured in a FTIR spectroscope with the Attenuated Total Reflection (ATR) method.[35] The measured absorbance spectrum of ES1 [blue solid line in Fig. 1(a)] shows an absorbance generally lower than $0.1\ \mu m^{-1}$ in the range from 600 to 2500 cm^{-1}, except for one sharp feature of $\sim 0.12\ \mu m^{-1}$ at 1490 cm^{-1}. Higher absorbance peaks of about $0.5\ \mu m^{-1}$ are visible below 3000 cm^{-1}. These peaks are attributed to the stretching vibrations of the $C_{sp3}-H_{x=1,2,3}$ groups present in tetraoctylphosphonium bromide.[36] Conversely, the absorbance spectrum of ES2 [red dashed line in Fig. 1(a)] shows more structured peaks up to $0.16\ \mu m^{-1}$ in the region from 600 to 2500 cm^{-1} and peaks around 3000 cm^{-1} lower with respect to ES1. These differences stem from the different cationic moiety of ES2, thus from the vibration modes of the imidazolium ring and from the stretching variation of the shorter aliphatic chain and of the $C_{sp2}-H$, respectively.[37] In both spectra, the peaks around 2350 cm^{-1} are due to the absorption of CO_2 in the atmosphere and are not related to the ILs.

We now focus on the ionic transport properties of ES1. To this scope, we fabricated metallic electrodes on top of boron-doped Si substrates covered with 300 nm of thermally grown SiO_2 by electron

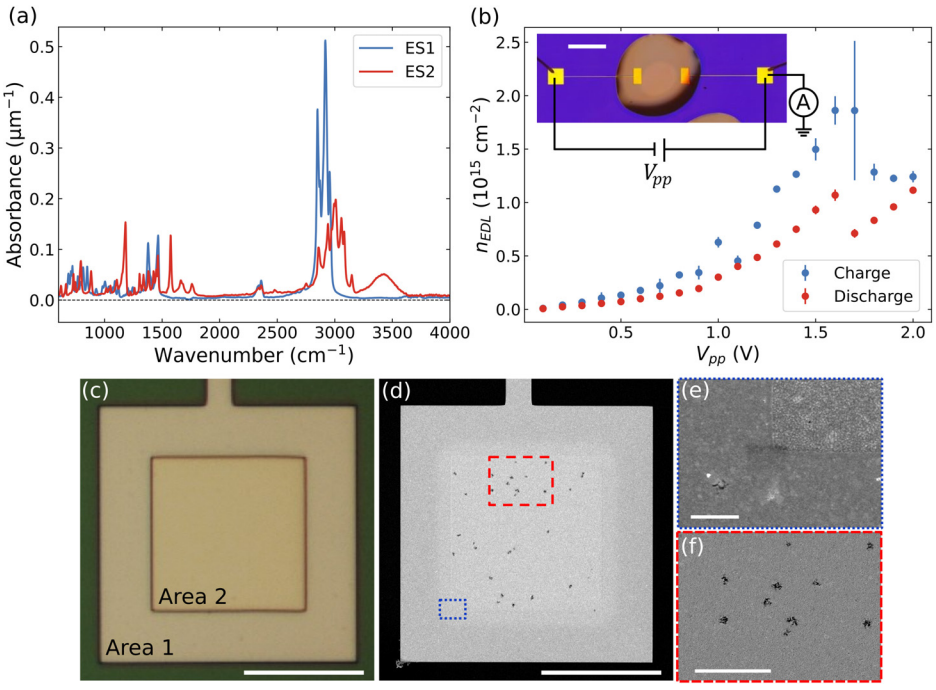

FIG. 1. (a) Absorbance spectra of ES1 (blue solid line) and ES2 (red dashed line). (b) Charging (n_{EDL}^{ch}, blue dots) and discharging (n_{EDL}^{dch}, red dots) carrier density accumulated in the EDL in a drop of ES1 vs V_{pp}. Inset: optical image of the IL droplet on the metal pads employed for the transport measurements along with the experimental setup. The scalebar is 500 μm. (c) Optical image of a pristine Cr/Au electrode. Area 1 is covered with a PMMA film, and Area 2 is exposed to air and will be in direct contact with ES1. The scalebar is 100 μm. (d) SEM image of the same electrode after the cycles of measurement in ambient conditions. The scalebar is 100 μm. (e) Detail of a region between Area 1 and Area 2 [blue dotted square in (d)]. The scalebar is 1 μm. (f) Detail of Area 2 [red dashed square in (d)]. The scalebar is 5 μm.

beam lithography (EBL) and thermal evaporation of 7 nm of chromium and 50 nm of gold [see the inset of Fig. 1(b)]. The transport properties of pure ES1 were investigated by Double Step Chronocoulometry[38] (DSC, see Fig. S2 in the supplementary material) in ambient conditions (with no control of environmental humidity and temperature). The accumulated charge in the EDL (Q_{EDL}) was determined both during its charging (*ch*) and discharging (*dch*) during two consecutive cycles. The two sets were averaged, their semi-dispersion used as error. Then, the values of Q_{EDL} were divided by the electrode area and by the electronic charge to extract the charge carrier density accumulated in (removed from) the EDL, i.e., n_{EDL}^{ch} (n_{EDL}^{dch}). Figure 1(b) reports n_{EDL}^{ch} and n_{EDL}^{dch} as a function of the applied potential (V_{pp}) for ES1 in air. The accumulated charge density grows with V_{pp} until reaching a value of $\sim 1.8 \times 10^{15} \mathrm{cm}^{-2}$ for $V_{pp} = 1.6$ V. For larger V_{pp}, the accumulated charge decreases. Such behavior is the result of the electrochemical activity of the system. Indeed, the upper limit of the electrochemical window[39] of ES1 is ~1.25 V when measured in air and ~1.8 V in vacuum (see Fig. S3 in the supplementary material). When the applied voltage exceeds such value, reduction/oxidation reactions start to take place at the interface between the liquid and the electrodes,[27,40] effectively reducing the charge accumulated in the EDL. Moreover, water from the atmosphere can dissolve in ES1. When applying a voltage bias, the absorbed water reacts with the bromide in the IL forming an acid environment.[41] Consequently, part of the Br^- anions involved in these reactions does not participate to the charging of the EDL. The electrochemical activity of the liquid generates a difference between the charging and the discharging of the EDL [red dots in Fig. 1(b)]. In particular, $Q_{EDL}^{ch} \sim 1.7 Q_{EDL}^{dch}$ for all values of $V_{pp} < 1.6$ V (see Fig. S4 in the supplementary material). This asymmetry can be partially linked to the mobility of the ions in the IL.[42] Indeed, the ions must overcome a barrier before starting to drift in the liquid. The applied bias both gives energy for the ions to exit the potential well and lowers the barrier to overcome.[43,44] When the potential is removed, the restored barrier yields lower charge removed in the same amount of time. The largest difference is observed for $V_{pp} = 1.7$ V, just above the electrochemical window limit. The anomalous error is attributed to a large difference between the two measurements for this bias value, indicating the onset of the electrochemical interactions. After this threshold, the asymmetry lowers as the voltage is increased because the reactions are less likely to occur in the discharge phase. This behavior suggests that, when the applied voltage is larger than the electrochemical barrier for the interaction, the change in the ionic mobility has, in fact, minor effects with respect to the chemical reactions.

To better understand the interaction between the liquid and the electrodes, the experiment was repeated on a device with electrodes partially covered by a PMMA with opening fabricated by EBL [see Fig. 1(c)]. After the transport measurements, ES1 and the PMMA mask were removed with acetone and the electrodes observed under a scanning electron microscope (SEM). The contrast between the two regions shows that the morphology of the metallic film that was in contact with ES1 is dramatically different from the one of the masked metal [see Fig. 1(d)], thus confirming that the IL chemically interacted with the electrodes. In addition, a 10-μm-wide transitional region is visible, due to the IL diffusion below the PMMA mask [see Fig. 1(e)]. In the region exposed to ES1, the overall roughness is increased, and holes are present in the metallic film [see Fig. 1(f)]. Such observation suggests that the electrochemically formed bromide-based acids attack the electrodes when applying a voltage. Indeed, the interaction of bromide with water absorbed from the atmosphere can create hypobromous acid (HOBr) and hydrobromic acid (HBr).[45] Both acids attack gold,[46] thus degrading the electrodes and reducing the gating effectiveness of the liquid. As a consequence, when voltages are applied to the liquid in ambient atmosphere, electrochemical reactions happen also within the electrochemical window. However, when water is removed from the liquid, the electrochemical window widens, and such reactions are avoided (see Fig. S3 in the supplementary material).

Since PMMA can absorb only a small amount of water (~2% w/w),[47] we exploit it to embed the bromide-based ILs and prevent the creation of an acid environment destructive for the devices. Furthermore, a spin-coated electrolyte thin film improves the device optical properties, thanks to its lower thickness and higher flatness. Therefore, we investigated both the optical and charge transport properties of the ILs when embedded in the PMMA matrix. To this scope, we synthesized two polymer electrolytes (PES1 and PES2) starting from ES1 and ES2. PES1 was produced by dissolving 4.30 mg of ES1 in 430 mg of AR 679.04 950 K (ethyl lactate solution of PMMA 950 K at 4%, AllResist), while PES2 was realized by dissolving 6.10 mg of ES2 in 612 mg of AR 679.04 950 K. Both solutions were therefore, 25% mg IL/mg PMMA. To demonstrate the suitability of PESs in optical experiments, we measured the optical transmission of a structure composed of a PES film spin-coated onto Si/SiO_2 substrates (4000 rpm for 1 min, soft baked at 100 °C for 2 min, thickness ~ 290 nm, see Fig. S1 in the supplementary material). In general, the PES/SiO_2/Si transmission spectra show a reduction of the transmitted power of ~5%–10% with respect to the bare substrate (see Fig. 2). This reduction is due to the absorption in the film and to reflection effects caused by the air/PES and PES/SiO_2 interfaces. The baseline is also influenced by thin film effects,[48] visible as a downward bending in the higher region of the spectra. Transmission dips related to PESs are present in the region 1200–1800 cm^{-1}. These lines are mainly attributed to the deformation

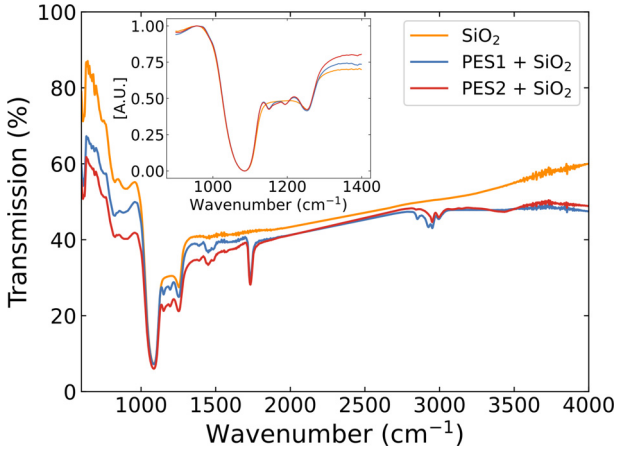

FIG. 2. Transmission spectrum of a Si/SiO_2 chip (orange line) compared to the transmission of the same substrate with PES1 (blue line) and PES2 (red line) on top. Inset: zoom of the signals in the region around the SiO_2 phonons. The minima were shifted to 0 and the signals normalized on their maxima for a better comparison of the shape.

vibrations of the (O)CH_3 and ester groups in the PMMA film[49] and are very similar for both PES1 and PES2. Instead, the two spectra differ in the region close to 3000 cm^{-1}, where the resonances are originated by the strain vibration of $CH_{x=1,2,3}$ groups.[50] Thus, the reduced transmission in the PESs film can be attributed to the different distribution of the $CH_{x=1,2,3}$ groups in the films due to the presence of the ESs. Nevertheless, the general features of the transmission spectrum of the bare substrate are preserved, such as the characteristic SiO_2 phonons at 1084 and 1256 cm^{-1},[51] see the inset of Fig. 2.

Generally, the charge transport properties of the electrolytes are modified when they are embedded in a polymer matrix,[52–56] especially when they are in the form of a thin film.[44] Indeed, the ionic transport is mediated by large molecules that migrate through the polymeric matrix. For example, amorphous polymers offer larger inter-molecular cavities for ions migration with respect to ordered polymers.[57] The dimension of inter-molecular cavities is also influenced by ion size[58] and by the employed solvent.[59] To test the suitability of our polymer electrolytes as gating materials, we performed DSC experiments on both PES1 and PES2. In the form of a thin film, PES1 showed a poor ionic transport due to the dimension and 3D structure of its cation, and, thus, we focused on PES2. Figure 3(a) shows the charge density accumulated in the EDL formed by a PES2 film as a function of the applied voltage V_{pp} both in ambient and vacuum conditions. In ambient conditions, the accumulated charge density reaches up to 2×10^{15} cm^{-2} for positive voltages and 4×10^{15} cm^{-2} for negative voltages [blue dots in Fig. 3(a)]. A nominally identical sample was investigated in vacuum at a pressure of $\sim 10^{-5}$ mbar [red dots in Fig. 3(a)]. The accumulated charge density is much higher in vacuum than in ambient pressure: $n_{EDL}^{vac}/n_{EDL}^{air} \sim 19.7$ for $V_{pp} = 0.5$ V and ~8.6 for $V_{pp} = -0.5$ V. The higher accumulated charge density in vacuum

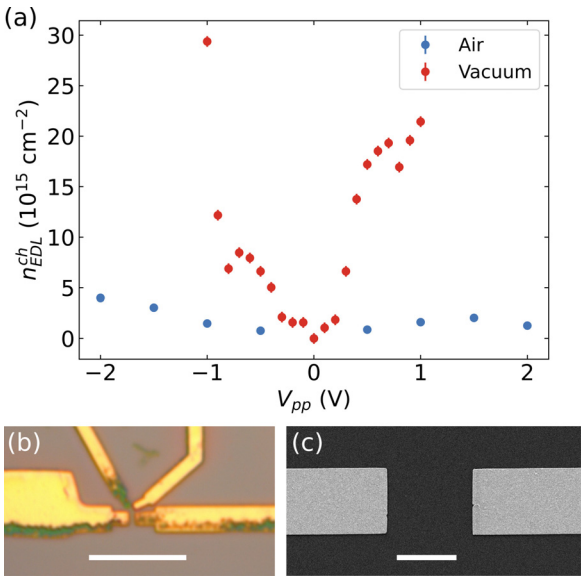

FIG. 3. (a) Charge density accumulated in the EDLs in PES2 when in ambient conditions (blue) and vacuum (orange) vs V_{pp}. (b) Optical image of the metallic electrodes employed for the measurement in ambient conditions. The scalebar is 5 μm. (c) SEM image of the metallic electrodes employed for measurement in vacuum. The scalebar is 10 μm.

is attributed to the increased ion mobility as a consequence of two concurring factors. First, when PESs are in vacuum, contaminant gaseous molecules such as water are expelled from the material. Second, the reduced pressure on the surface allows for the structure to relax, thus creating wider paths for ions to migrate. The asymmetry measured for positive and negative values of the applied potential in vacuum can be attributed to the different nature of the anion and the cation, both in terms of chemistry, for example, the distinct tendency to share or not electrons (thus lowering or not the potential barrier for their diffusion[43]), and in terms of dimensions; in fact, the molecular mass and the volume influence the ion stability once a potential is applied (i.e., the selected anions are lighter and smaller than cations) and its ability to move across the polymer matrix.[31] Similarly to pure ES1 [see Fig. 1(b)], the induced charge density grows following a monotonic trend until $|V_{pp}| \sim 0.9$ V. After that threshold, the ions in the electrolyte start interacting with the polymer matrix and the electrodes, thus modifying the EDL charging efficiency.

Despite the IL being embedded in PMMA, an acid environment is created when applying a DC bias to PES2 in ambient conditions, as measured for bare ES1 [see Figs. 1(c)–1(f)]. This acid environment modifies the morphology of the device electrodes, as clearly observable in Fig. 3(b). Conversely, when PES2 is measured in vacuum, the electrodes are preserved from electrochemical damaging [Fig. 3(c)]. This indicates the small amount of water trapped by the PMMA film in ambient conditions is sufficient to create HOBr and/or HBr. Instead, in vacuum, the film expels most of the absorbed water, thus preventing the formation of the acid environment.

After removing the water by keeping the device in vacuum, we tested the stability of the PES structure by performing consecutive DSC cycles with a fixed $V_{pp} = 300$ mV in ambient conditions. As shown in Fig. 4(a), the accumulated charge density n_{EDL}^{N} is highly stable for the first six cycles. Here, n_{EDL}^{N} is the accumulated charge density at cycle N normalized by the carrier concentration accumulated during the first cycle. After these cycles, n_{EDL}^{N} increases of a factor ~1.3. This increase can be tentatively explained by considering that, when the polymer is brought back at air conditions, the reduction of polymer film volume caused by the air pressure leads to a decrease in the paths for the ions migration. Consequently, during the first few cycles, the ions are pushed through the polymer matrix and open back accessible paths for the charge migration. As a result, the charge accumulated in the EDL increases after a few cycles, as similarly occurs for lithium intercalation in bilayer graphene.[60,61] It is worth notice that, differently from previous experiments, the applied potential does not damage the electrodes, as shown in Fig. 4(b). Interestingly, the macroscopic morphology of the PES2 film changes after the application of voltages in ambient conditions after the vacuum treatment. Indeed, bias-induced cracks appear over the surface of the polymer, mainly starting from points where the film was already damaged, such as near the bonding wires or metallic residues [see Figs. 4(b) and S5 in the supplementary material). Indeed, the water molecules can efficiently penetrate into the PMMA film from these points. Within these cracks, Br-based acids can be electrochemically created and gradually diffuse through the polymer matrix. In full agreement with the DSC measurements, Fig. 4(b) shows that even when the cracks are formed, the electrodes are not degraded, suggesting that negligible chemical interactions took place. Therefore, removing the water content from the polymer matrix before any voltage is applied enhances the robustness of polymer-

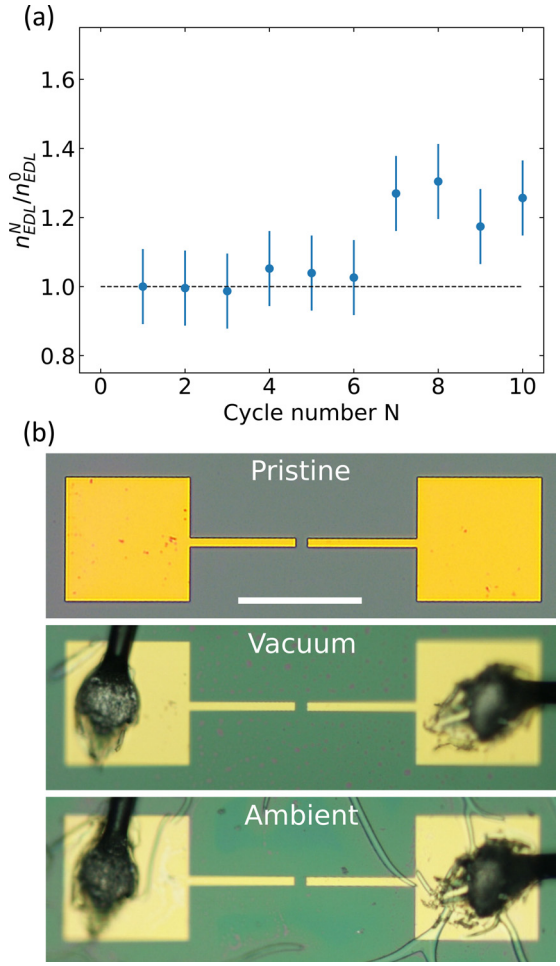

FIG. 4. (a) Charge density accumulated in consecutive cycles performed on PES2 in ambient conditions at $V_{pp} = 300$ mV after the measurements in vacuum. (b) Optical images of the metallic pads used in the chronocoulometry measurements before PES2 is spinned (top), after the measurement in vacuum (middle) and after the measurement in air (bottom). The scalebar is 150 μm. The bonding wires used for electrical measurements are visible on the gold pads in the middle and bottom images.

embedded ionic liquids. Indeed, a simple treatment in vacuum preparation ensures a large stability of the accumulated charge density and prevents the formation of an acid environment in the proximity of the metallic electrodes even when employed for several cycles in air. In summary, we proposed and demonstrated the optical and transport properties of a class of polymer-embedded ionic liquids based on bromide. The EDLs that form when the films are polarized can accumulate state-of-the-art charge densities up to $\sim 20 \times 10^{15}$ cm^{-2} in vacuum.[15] Furthermore, these electrolytes are transparent in the mid-infrared region of the spectrum and can be easily spin-coated in the form of a thin film, thus providing remarkable advantages in optoelectronic devices. Although bromide-based ILs react with water to form acids chemically attacking the electrodes, we demonstrated that it is possible to remove the absorbed water by a vacuum treatment before any voltage is applied, thus preventing the degradation of the metals. Furthermore, the polymer matrix of PMMA embedded ILs protects the electrodes for several cycles in ambient conditions after the vacuum curing. Therefore, devices exploiting our electrolytes can be fabricated with standard techniques in ambient conditions without the need of the inert atmosphere of a glovebox, as usually necessary for lithium-based ILs.[18,19,60,61]

See the supplementary material for additional details on the methods employed, supporting data on thickness and electrochemical windows of the electrolytes, and additional optical and SEM images of the devices exploited in this study.

Fe.B. acknowledges the project q-LIMA in the framework of the PRIN2020 initiative of the Italian Ministry of University and Research for partial financial support. Gio.T., A.M., L.G., C.S.P., and S.R. acknowledge the project Quantum2D in the framework of the PRIN2017 initiative of the Italian Ministry of University and Research for partial financial support.

AUTHOR DECLARATIONS

Conflict of Interest

The authors have no conflicts to disclose.

Author Contributions

Nicola Melchioni: Data curation (lead); Formal analysis (lead); Investigation (equal); Writing – original draft (lead). **Stefano Roddaro:** Conceptualization (equal); Resources (equal); Supervision (supporting). **Alessandro Tredicucci:** Conceptualization (equal); Resources (equal); Supervision (equal); Validation (equal); Writing – review & editing (equal). **Federico Paolucci:** Conceptualization (lead); Resources (equal); Supervision (lead); Writing – review & editing (lead). **Giacomo Trupiano:** Data curation (equal); Investigation (equal). **Giorgio Tofani:** Data curation (equal); Investigation (equal); Writing – original draft (equal). **Riccardo Bertini:** Formal analysis (supporting); Investigation (supporting). **Andrea Mezzetta:** Investigation (equal); Methodology (equal). **Federica Bianco:** Funding acquisition (equal); Investigation (equal); Writing – review & editing (equal). **Lorenzo Guazzelli:** Methodology (equal); Validation (equal). **Fabio Beltram:** Resources (lead). **Christian Silvio Pomelli:** Methodology (equal); Resources (equal); Supervision (equal).

DATA AVAILABILITY

The data that support the findings of this study are available from the corresponding author upon reasonable request.

REFERENCES

[1]H. Yan, F. Xia, W. Zhu, M. Freitag, C. Dimitrakopoulos, A. A. Bol, G. Tulevski, and P. Avouris, "Infrared spectroscopy of wafer-scale graphene," ACS Nano **5**, 9854–9860 (2011).
[2]A. Grigorenko, M. Polini, and K. Novoselov, "Graphene plasmonics," Nat. Photonics **6**, 749–758 (2012).
[3]J. B. Oostinga, H. B. Heersche, X. Liu, A. F. Morpurgo, and L. M. K. Vandersypen, "Gate-induced insulating state in bilayer graphene devices," Nat. Mater. **7**, 151–157 (2008).
[4]Y. Zhang, T.-T. Tang, C. Girit, Z. Hao, M. C. Martin, A. Zettl, M. F. Crommie, R. Shen, and F. Wang, "Direct observation of a widely tunable bandgap in bilayer graphene," Nature **459**, 820–823 (2009).

[5]X. Dai, W. Li, T. Wang, X. Wang, and C. Zhai, "Bandstructure modulation of two-dimensional WSe_2 by electric field," J. Appl. Phys. **117**, 084310 (2015).
[6]J. Kim, S. S. Baik, S. H. Ryu, Y. Sohn, S. Park, B.-G. Park, J. Denlinger, Y. Yi, H. J. Choi, and K. S. Kim, "Observation of tunable band gap and anisotropic Dirac semimetal state in black phosphorus," Science **349**, 723–726 (2015).
[7]C. Forsythe, X. Zhou, K. Watanabe, T. Taniguchi, A. Pasupathy, P. Moon, M. Koshin, P. Kim, and C. R. Dean, "Band structure engineering of 2D materials using patterned dielectric superlattices," Nat. Nanotechnol. **13**, 566–571 (2018).
[8]P. Chen, C. Cheng, C. Shen, J. Zhang, S. Wu, X. Lu, S. Wang, L. Du, K. Watanabe, T. Taniguchi, J. Sun, R. Yang, D. Shi, K. Liu, S. Meng, and G. Zhang, "Band evolution of two-dimensional transition metal dichalcogenides under electric fields," Appl. Phys. Lett. **115**, 083104 (2019).
[9]M. C. Lemme, T. J. Echtermeyer, M. Baus, and H. Kurz, "A graphene field-effect device," IEEE Electron Device Lett. **28**, 282–284 (2007).
[10]L. A. W. Robinson, S.-B. Lee, K. B. K. Teo, M. Chhowalla, G. A. J. Amaratunga, W. I. Milne, D. A. Williams, D. G. Hasko, and H. Ahmed, "Fabrication of self-aligned side gates to carbon nanotubes," Nanotechnology **14**, 290 (2003).
[11]K. S. Novoselov, A. Mishchenko, A. Carvalho, and A. H. C. Neto, "2D materials and van der Waals heterostructures," Science **353**, aac9439 (2016).
[12]C. Lu, Q. Fu, S. Huang, and J. Liu, "Polymer electrolyte-gated carbon nanotube field-effect transistor," Nano Lett. **4**, 623–627 (2004).
[13]R. Misra, M. McCarthy, and A. F. Hebard, "Electric field gating with ionic liquids," Appl. Phys. Lett. **90**, 052905 (2007).
[14]K. Segawa, Z. Ren, S. Sasaki, T. Tsuda, S. Kuwabata, and Y. Ando, "Ambipolar transport in bulk crystals of a topological insulator by gating with ionic liquid," Phys. Rev. B **86**, 075306 (2012).
[15]E. Piatti, "Ionic gating in metallic superconductors: A brief review," Nano Express **2**, 024003 (2021).
[16]T. Fujimoto and K. Awaga, "Electric-double-layer field-effect transistors with ionic liquids," Phys. Chem. Chem. Phys. **15**, 8983–9006 (2013).
[17]H. Zhang, C. Berthod, H. Berger, T. Giamarchi, and A. F. Morpurgo, "Band filling and cross quantum capacitance in ion-gated semiconducting transition metal dichalcogenide monolayers," Nano Lett. **19**, 8836–8845 (2019).
[18]R. S. Gonnelli, E. Piatti, A. Sola, M. Tortello, F. Dolcini, S. Galasso, J. R. Nair, C. Gerbaldi, E. Cappelluti, M. Bruna, and A. C. Ferrari, "Weak localization in electric-double-layer gated few-layer graphene," 2D Mater. **4**, 035006 (2017).
[19]D. Daghero, F. Paolucci, A. Sola, M. Tortello, G. A. Ummarino, M. Agosto, R. S. Gonnelli, J. R. Nair, and C. Gerbaldi, "Large conductance modulation of gold thin films by huge charge injection via electrochemical gating," Phys. Rev. Lett. **108**, 066807 (2012).
[20]B. I. Weintrub, Y.-L. Hsieh, S. Kovalchuk, J. N. Kirchhof, K. Greben, and K. I. Bolotin, "Generating intense electric fields in 2D materials by dual ionic gating," Nat. Commun. **13**, 6601 (2022).
[21]J. T. Ye, Y. J. Zhang, R. Akashi, M. S. Bahramy, R. Arita, and Y. Iwasa, "Superconducting dome in a gate-tuned band insulator," Science **338**, 1193–1196 (2012).
[22]S. Wang, M. Ha, M. Manno, C. D. Frisbie, and C. Leighton, "Hopping transport and the Hall effect near the insulator–metal transition in electrochemically gated poly(3-hexylthiophene) transistors," Nat. Commun. **3**, 1210 (2012).
[23]E. Ponomarev, N. Ubrig, I. Gutiérrez-Lezama, H. Berger, and A. F. Morpurgo, "Semiconducting van der Waals interfaces as artificial semiconductors," Nano Lett. **18**, 5146–5152 (2018).
[24]D. Domaretskiy, M. Philippi, M. Gibertini, N. Ubrig, I. Gutiérrez-Lezama, and A. F. Morpurgo, "Quenching the bandgap of two-dimensional semiconductors with a perpendicular electric field," Nat. Nanotechnol. **17**, 1078–1083 (2022).
[25]M. P. Murrell, M. E. Welland, S. J. O'Shea, T. M. H. Wong, J. R. Barnes, A. W. McKinnon, M. Heyns, and S. Verhaverbeke, "Spatially resolved electrical measurements of SiO_2 gate oxides using atomic force microscopy," Appl. Phys. Lett. **62**, 786–788 (1993).
[26]Y. Hattori, T. Taniguchi, K. Watanabe, and K. Nagashio, "Anisotropic dielectric breakdown strength of single crystal hexagonal boron nitride," ACS Appl. Mater. Interfaces **8**, 27877–27884 (2016).
[27]S. Zhao, Z. Zhou, B. Peng, M. Zhu, M. Feng, Q. Yang, Y. Yan, W. Ren, Z.-G. Ye, Y. Liu, and M. Liu, "Quantitative determination on ionic-liquid-gating control of interfacial magnetism," Adv. Mater. **29**, 1606478 (2017).
[28]L. Sheng, Q. Wang, X. Liu, H. Cui, X. Wang, Y. Xu, Z. Li, L. Wang, Z. Chen, G. Xu, J. Wang, Y. Tang, K. Amine, H. Xu, and X. He, "Suppressing electrolyte-lithium metal reactivity via Li^+-desolvation in uniform nano-porous separator," Nat. Commun. **13**, 172 (2022).
[29]C. Ferdeghini, L. Guazzelli, C. S. Pomelli, A. Ciccioli, B. Brunetti, A. Mezzetta, and S. Vecchio Ciprioti, "Synthesis, thermal behavior and kinetic study of n-morpholinium dicationic ionic liquids by thermogravimetry," J. Mol. Liq. **332**, 115662 (2021).
[30]M. Vraneš, S. Papović, S. Rackov, K. Alenezi, S. Gadžurić, A. Tot, and B. Pilić, "Thermophysical and electrochemical properties of 1-alkyl-3–(3-butenyl)imidazolium bromide ionic liquids," J. Chem. Thermodyn. **139**, 105871 (2019).
[31]E. Piatti, L. Guglielmero, G. Tofani, A. Mezzetta, L. Guazzelli, F. D'Andrea, S. Roddaro, and C. S. Pomelli, "Ionic liquids for electrochemical applications: Correlation between molecular structure and electrochemical stability window," J. Mol. Liq. **364**, 120001 (2022).
[32]O. Palumbo, A. Cimini, F. Trequattrini, J.-B. Brubach, P. Roy, and A. Paolone, "The infrared spectra of protic ionic liquids: Performances of different computational models to predict hydrogen bonds and conformer evolution," Phys. Chem. Chem. Phys. **22**, 7497–7506 (2020).
[33]T. Moumene, E. H. Belarbi, B. Haddad, D. Villemin, O. Abbas, B. Khelifa, and S. Bresson, "Vibrational spectroscopic study of ionic liquids: Comparison between monocationic and dicationic imidazolium ionic liquids," J. Mol. Struct. **1065–1066**, 86–92 (2014).
[34]C. Chiappe, A. Mezzetta, C. S. Pomelli, M. Puccini, and M. Seggiani, "Product as reaction solvent: An unconventional approach for ionic liquid synthesis," Org. Process Res. Dev. **20**, 2080–2084 (2016).
[35]A. Mendoza-Galván, J. Méndez-Lara, R. Mauricio-Sánchez, K. Järrendahl, and H. Arwin, "Effective absorption coefficient and effective thickness in attenuated total reflection spectroscopy," Opt. Lett. **46**, 872–875 (2021).
[36]R. M. Silverstein, F. X. Webster, D. J. Kiemle, and D. L. Bryce, *Spectrometric Identification of Organic Compounds*, 8th ed. (Wiley, 2014).
[37]T. Yamada, Y. Tominari, S. Tanaka, and M. Mizuno, "Infrared spectroscopy of ionic liquids consisting of imidazolium cations with different alkyl chain lengths and various halogen or molecular anions with and without a small amount of water," J. Phys. Chem. B **121**, 3121–3129 (2017).
[38]G. Inzelt, "Chronocoulometry," in *Electroanalytical Methods: Guide to Experiments and Applications*, edited by F. Scholz, A. Bond, R. Compton, D. Fiedler, G. Inzelt, H. Kahlert, Š. Komorsky-Lovrić, H. Lohse, M. Lovrić, F. Marken, A. Neudeck, U. Retter, F. Scholz, and Z. Stojek (Springer Berlin Heidelberg, Berlin, Heidelberg, 2010), pp. 147–158.
[39]M. Hayyan, F. S. Mjalli, M. A. Hashim, I. M. AlNashef, and T. X. Mei, "Investigating the electrochemical windows of ionic liquids," J. Ind. Eng. Chem. **19**, 106–112 (2013).
[40]H. H. Girault, *Analytical and Physical Electrochemistry*, 1st ed. (EPFL Press, 2004).
[41]I. A. Shkrob, T. W. Marin, R. A. Crowell, and J. F. Wishart, "Photo- and radiation-chemistry of halide anions in ionic liquids," J. Phys. Chem. A **117**, 5742–5756 (2013).
[42]R. Clark, M. von Domaros, A. J. S. McIntosh, A. Luzar, B. Kirchner, and T. Welton, "Effect of an external electric field on the dynamics and intramolecular structures of ions in an ionic liquid," J. Chem. Phys. **151**, 164503 (2019).
[43]R. Shi and Y. Wang, "Ion-cage interpretation for the structural and dynamic changes of ionic liquids under an external electric field," J. Phys. Chem. B **117**, 5102–5112 (2013).
[44]Q. Zhao, P. Bennington, P. F. Nealey, S. N. Patel, and C. M. Evans, "Ion specific, thin film confinement effects on conductivity in polymerized ionic liquids," Macromolecules **54**, 10520–10528 (2021).
[45]J. D. Sivey, J. S. Arey, P. R. Tentscher, and A. L. Roberts, "Reactivity of BrCl, Br_2, BrOCl, Br_2O, and HOBr toward dimethenamid in solutions of bromide + aqueous free chlorine," Environ. Sci. Technol. **47**, 1330–1338 (2013).
[46]P. Walker and W. H. Tarn, *CRC Handbook of Metal Etchants* (CRC Press, 1990).
[47]M. N'Diaye, F. Pascaretti-Grizon, P. Massin, M. F. Baslé, and D. Chappard, "Water absorption of poly(methyl methacrylate) measured by vertical interference microscopy," Langmuir **28**, 11609–11614 (2012).
[48]E. El-Menyawy, N. El-Ghamaz, and H. Nawar, "Infrared spectra, optical constants and semiconductor behavior of 5–(2-phenylhydrazono)-3,3-dimethylcyclohexanone thin films," J. Mol. Struct. **1036**, 144–150 (2013).

[49]S. Jitian and I. Bratu, "Determination of optical constants of polymethyl methacrylate films from IR reflection-absorption spectra," AIP Conf. Proc. **1425**, 26–29 (2012).
[50]Y. Jeon, J. Sung, C. Seo, H. Lim, H. Cheong, M. Kang, B. Moon, Y. Ouchi, and D. Kim, "Structures of ionic liquids with different anions studied by infrared vibration spectroscopy," J. Phys. Chem. B **112**, 4735–4740 (2008).
[51]A. Lehmann, L. Schumann, and K. Hübner, "Optical phonons in amorphous silicon oxides. I. Calculation of the density of states and interpretation of Lo-To splittings of amorphous SiO_2," Phys. Status Solidi B **117**, 689–698 (1983).
[52]S. Mogurampelly and V. Ganesan, "Structure and mechanisms underlying ion transport in ternary polymer electrolytes containing ionic liquids," J. Chem. Phys. **146**, 074902 (2017).
[53]V. Ganesan, "Ion transport in polymeric ionic liquids: Recent developments and open questions," Mol. Syst. Des. Eng. **4**, 280–293 (2019).
[54]N. M. Vargas-Barbosa and B. Roling, "Dynamic ion correlations in solid and liquid electrolytes: How do they affect charge and mass transport?," ChemElectroChem **7**, 367–385 (2020).
[55]W. Xiao, Q. Yang, and S. Zhu, "Comparing ion transport in ionic liquids and polymerized ionic liquids," Sci. Rep. **10**, 7825 (2020).
[56]K. D. Fong, J. Self, B. D. McCloskey, and K. A. Persson, "Ion correlations and their impact on transport in polymer-based electrolytes," Macromolecules **54**, 2575–2591 (2021).
[57]S. Ramesh, C.-W. Liew, and K. Ramesh, "Evaluation and investigation on the effect of ionic liquid onto PMMA-PVC gel polymer blend electrolytes," J. Non-Cryst. Solids **357**, 2132–2138 (2011).
[58]K.-H. Shen and L. M. Hall, "Effects of ion size and dielectric constant on ion transport and transference number in polymer electrolytes," Macromolecules **53**, 10086–10096 (2020).
[59]S. Sharick, J. Koski, R. A. Riggleman, and K. I. Winey, "Isolating the effect of molecular weight on ion transport of non-ionic diblock copolymer/ionic liquid mixtures," Macromolecules **49**, 2245–2256 (2016).
[60]M. Kühne, F. Paolucci, J. Popovic, P. Ostrovsky, J. Maier, and J. Smet, "Ultrafast lithium diffusion in bilayer graphene," Nat. Nanotechnol. **12**, 895–900 (2017).
[61]P. Zielinski, M. Kühne, D. Kärcher, F. Paolucci, P. Wochner, S. Fecher, J. Drnec, R. Felici, and J. H. Smet, "Probing exfoliated graphene layers and their lithiation with microfocused x-rays," Nano Lett. **19**, 3634–3640 (2019).